iScience

CellPress
OPEN ACCESS

Article

Nuclear transfer improves the developmental potential of embryos derived from cytoplasmic deficient oocytes

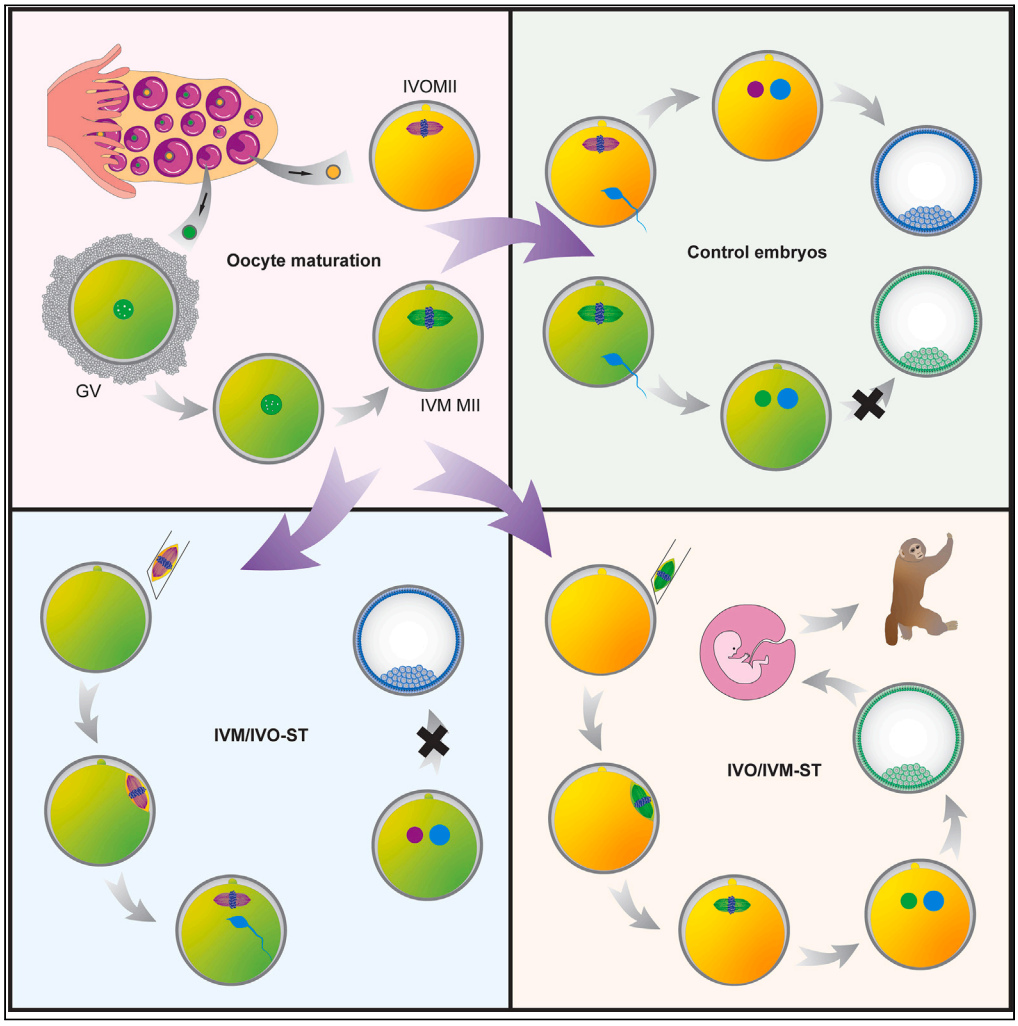

Zhaodi Liao,
Yuzhuo Li,
Chunyang Li,
Xinyan Bian,
Qiang Sun

qsun@ion.ac.cn

Highlights

Spindle-chromosome complex transfer improves cytoplasmic quality of primate oocytes

In vitro matured oocyte nuclei support pre- and post-implantation embryo development

Live rhesus monkeys were obtained by nucleus transferred of *in vitro* matured oocyte

Liao et al., iScience *26*, 107299
August 18, 2023
https://doi.org/10.1016/j.isci.2023.107299

iScience

CellPress
OPEN ACCESS

Article

Nuclear transfer improves the developmental potential of embryos derived from cytoplasmic deficient oocytes

Zhaodi Liao,[1,2,3] Yuzhuo Li,[1,2] Chunyang Li,[1,2] Xinyan Bian,[1,2] and Qiang Sun[1,2,4,*]

SUMMARY

Embryo development after fertilization is largely determined by the oocyte quality, which is in turn dependent on the competence of both the cytoplasm and nucleus. Here, to improve the efficiency of embryo development from developmentally incompetent oocytes, we performed spindle-chromosome complex transfer (ST) between *in vitro* matured (IVM) and *in vivo* matured (IVO) oocytes of the non-human primate rhesus monkey. We observed that the blastocyst rate of embryos derived from transferring the spindle-chromosome complex (SCC) of IVM oocytes into enucleated IVO oocytes was comparable with that of embryos derived from IVO oocytes. After transferring the reconstructed embryos into the uterus of surrogate mothers, two live rhesus monkeys were obtained, indicating that the nuclei of IVM oocytes support both the pre-and post-implantation embryo development of non-human primates.

INTRODUCTION

A developmentally competent oocyte is a prerequisite for normal pre- and post-implant development of the fertilized egg. However, oocyte quality can be affected by aging,[1,2] impaired maturation,[3] genetic mutations,[4] and various other factors that impair either the cytoplasm or nucleus or both. Although many studies have focused on promoting the efficiency of embryo development from low-quality oocytes, limited success has been achieved.

In vitro maturation (IVM) has been adopted for the treatment of women suffering from polycystic ovary syndrome (PCOS) or ovarian hyperstimulation syndrome (OHSS) and women who have a limited time window for fertility protection before the radiotherapy and chemotherapy of cancers.[5–8] Because of the asynchronous maturation of the nucleus and cytoplasm, the cytoplasm quality of oocytes derived from IVM is inferior compared with that of oocytes obtained from conventional hormone-stimulated assisted reproductive technology.[3,5,9] Despite this drawback, IVM has been adopted clinically, and efforts have been made to improve the cytoplasm quality. Although some antioxidants have been identified and added to the IVM culture media, the fertilization, cleavage, and blastocyst rates of these IVM oocytes are still lower than those of *in vivo* matured (IVO) oocytes retrieved from the patient.[10]

On the other hand, the feasibility of nuclear transfer technologies, including germinal vesicle transfer (GVT),[11] spindle-chromosome complex transfer (ST),[12–16] pronuclear transfer (PNT),[17,18] and polar body transfer (PBT),[19–21] have been demonstrated in primates. So far, there has been no obvious reduction in the fertilization and developmental efficiency observed in normally fertilized nuclear transferred embryos compared with non-transfer control embryos. More importantly, no detrimental defects have been identified in nuclear transfer embryos or surviving infants after birth.[12,15,21]

Defects in cytoplasmic maturation have been frequently reported to lead to embryo development failure; therefore, we investigated whether the developmental competency of cytoplasmic-deficient oocytes can be improved by transferring nuclei from IVM oocytes (IVM MIIs) to enucleated IVO oocytes (IVO MIIs) in the non-human primate the rhesus monkey. Cumulus cells play a vital role during the oocyte maturation process, and several studies have reported that cumulus cell denudation significantly impairs oocyte maturation and subsequent developmental competency.[22–28] Therefore, to obtain low-quality oocytes, we collected cumulus-denuded germinal vesicle (GV) oocytes from rhesus monkeys after each trial of

[1]Institute of Neuroscience, Center for Excellence in Brain Science and Intelligence Technology, State Key Laboratory of Neuroscience, Chinese Academy of Sciences, Shanghai 200031, China

[2]Shanghai Center for Brain Science and Brain-Inspired Technology, Shanghai 201210, China

[3]University of Chinese Academy of Sciences, Beijing 100049, China

[4]Lead contact

*Correspondence: qsun@ion.ac.cn

https://doi.org/10.1016/j.isci.2023.107299

conventional stimulated superovulation for *in vitro* maturation. The denuded oocytes underwent regular GV breakdown and were reached to the metaphase of the second meiosis (MII) as indicated by the appearance of the first polar body (PB1). We thus transferred the SCCs from IVM oocytes into enucleated IVO oocytes and obtained nuclear transferred oocytes for intracytoplasmic sperm injection. The blastocyst and birth rates were comparable between embryos derived from nuclear transfer and normal fertilization, indicating that nuclear transfer provides a new way for obtaining offspring using oocytes with incompetent cytoplasm.

RESULTS

Cytoplasmic incompetence leads to IVM failure

Here, in this study, we adopted a previously reported IVM method for capturing the low-quality oocytes.[29] We observed a maturation rate of 54.5% when cumulus cell-denuded monkey GV oocytes were matured *in vitro* (Table S1). However, the programmed synchronized maturation of the oocyte nucleus and cytoplasm was disrupted by the deletion of cumulus cells and surrounding follicular fluids *in vitro*. Thus, the developmental competency of the embryos derived from IVM MIIs was significantly lower compared with that of embryos derived from IVO MIIs (0% vs. 68%, Figures 1A and S1A).

We next performed RNA sequencing (RNA-seq) using GV, IVM MIIs, and IVO MIIs, and compared their gene expression. There was good reproducibility between biological replicates, and we found that the samples from each type of oocyte were distinct from the others as observed in principle component analysis (Figures 1B and S2A). The distinction between IVM MIIs and IVO MIIs was also demonstrated by Spearman correlation analysis (Figure S2B). We identified a total of 8,103 differentially expressed genes (DEGs) between GV, IVM MIIs, and IVO MIIs using stringent criterion (FoldChange >2, p value <0.01, baseMean >10, Figures 1C, S2C, and S2D). These DEGs were then classified into eight clusters using unsupervised hierarchical cluster analysis (Figure 1D). Clusters 2, 7 and 8 contained genes that were identified as upregulated in IVM MIIs compared with IVO MIIs, whereas genes in clusters 3, 4, and 5 were identified as downregulated in IVM oocytes. Gene ontology analysis indicated that clusters 2, 7, and 8 were mainly enriched in pathways related to mitochondrial regulation, whereas clusters 3, 4, and 5 were enriched in pathways related to nuclear division, RNA splicing and chromosome segregation (Figure 1E).

Mitochondria are important for ATP production, and their distribution and copy number in cytoplasm was previously reported to be critical for oocyte competence.[3,30] To further confirm that IVM MIIs obtained using denuded GVs were developmentally incompetent in our study, we next investigated mitochondrial repositioning in the cytoplasm during IVM. We observed that the mitochondria were peripherally positioned and centrally located in the GV and IVO MIIs, respectively, whereas they were located in both the peripheral and center areas of the IVM cytoplasm (Figure S1B). Comparison of the fluorescence intensities of mitochondria stained with MitoTracker between the "center" and "edge" areas of the oocytes confirmed that the IVM MIIs more closely resembled an intermediate state in the transition of GV to IVO MIIs (Figure S1C). Consistent with the upregulation of mitochondrial genes in IVM MIIs, we found that the copy number of mitochondria genomes (mtDNA) was higher in IVM MII oocytes than in IVO MII oocytes (3.46×10^6 vs. 2.37×10^6, Figure S1D).

Proper epigenetic modification occurs in IVM oocytes

We next examined the nuclear integrity, epigenetic modifications, and organelle reorganization in the IVM MIIs. By co-staining DNA together with ∂-tubulin (one of the subunits of tubulin) and phosphorylated histone H3, we found that the chromosomes were well located on the spindle plate, indicating that the genome structure was morphologically similar between IVM and IVO MIIs (Figure 2A). Next, we compared the gene expression level of key epigenetic modification factors (FPKM >1) using the RNA sequencing data generated in this study. The results showed that all of the DNA methylation, histone methylation and histone acetylation factors showed comparable expression levels between IVM and IVO MIIs (Figure 2B). This result was also confirmed by immunostaining, as histone H3 trimethyl K4 (H3K4me3), histone H3 trimethyl K9 (H3K9me3), histone H3 trimethyl K27 (H3K27me3), and DNA methylation in IVM MIIs were all demonstrated to be comparable with those in IVO MIIs (Figures 2C–2F).

These data indicated that IVM MIIs did not show any alterations in nuclear integrity or epigenetic modifications compared with IVO MIIs.

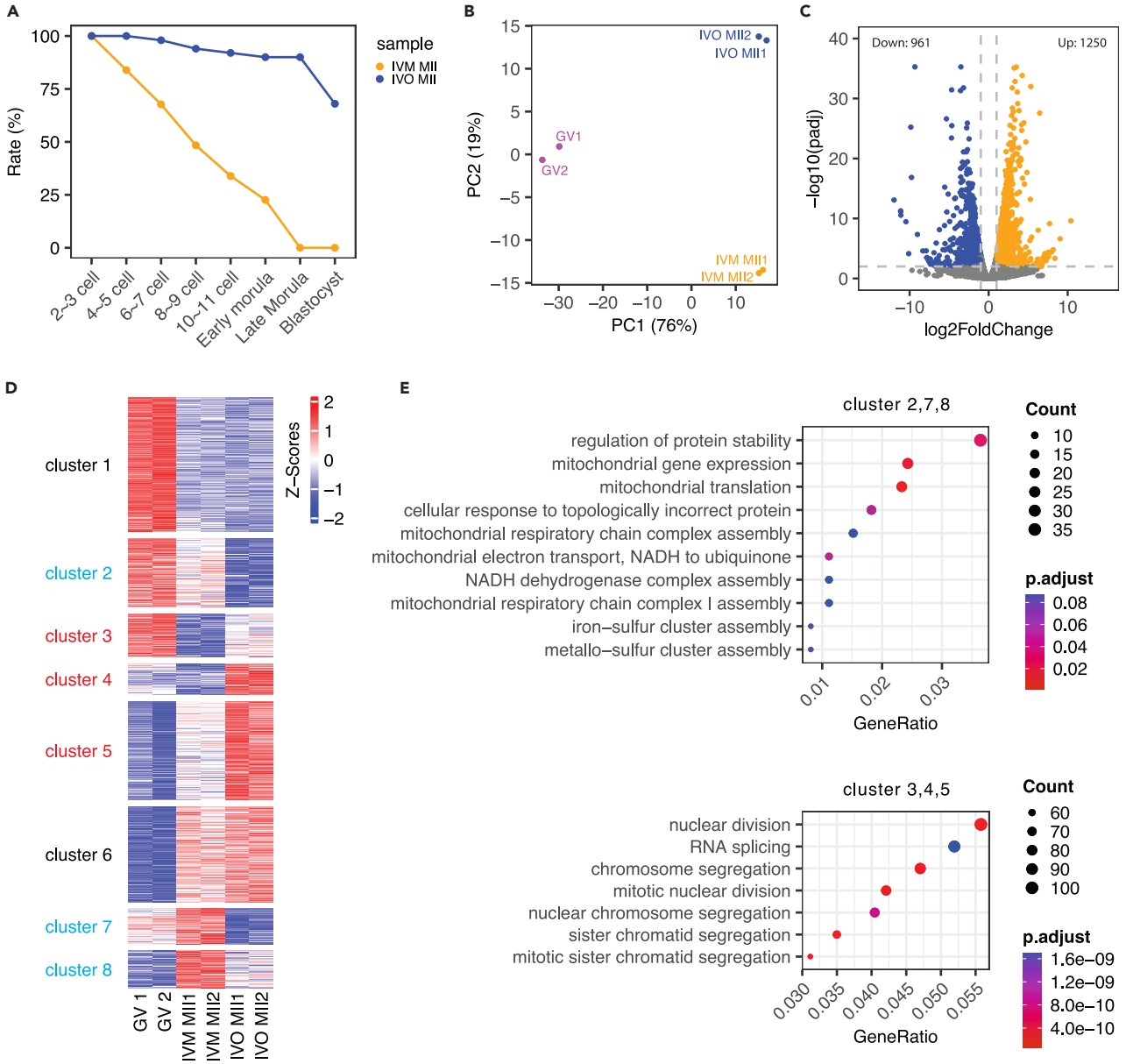

Figure 1. Developmental competence of IVM oocytes

(A) Pre-implant developmental competency of embryos derived from IVM (orange) and IVO (blue) oocytes in different embryonic stages. The embryo development stage shown on the x axis was assigned according to the number of blastomeres.

(B) Principal component analysis (PCA) of the RNA-seq data for GV, IVM, and IVO oocytes. GV, IVM, and IVO oocytes formed distinct clusters.

(C) Volcano plot showing the differentially expressed genes (DEGs) between IVM and IVO oocytes. Up (orange): genes upregulated in IVM oocytes compared with IVO oocytes; Down (blue): genes downregulated in IVM oocytes compared with IVO oocytes.

(D) Heatmap showing 8,103 DEGs (FoldChange >2, p value <0.01, baseMean >10) derived from pairwise comparisons between GV, IVM, and IVO oocytes. The genes were classified into eight clusters using unsupervised hierarchical clustering. The gene expression level was colored from blue to white to red to indicate low, medium and high expression. Cluster 2, 7 and 8 were classified into a new group (indicated in blue), while clusters 3, 4, and 5 were grouped together (indicated in red).

(E) Gene ontology analysis of the genes in clusters 2, 7 and 8 (up) and clusters 3, 4 and 5 (down) from (D).

Nuclei of IVM oocytes direct normal embryonic development in IVO oocyte cytoplasm

Next, we combined the methods of IVM and nuclear transfer to investigate whether the nucleus of IVM MIIs could be used to generate viable offspring (Figures 3A and 3B). Here, the oocytes reconstructed by combining enucleated IVO oocytes with IVM SCCs were named IVO/IVM-ST oocytes, and oocytes

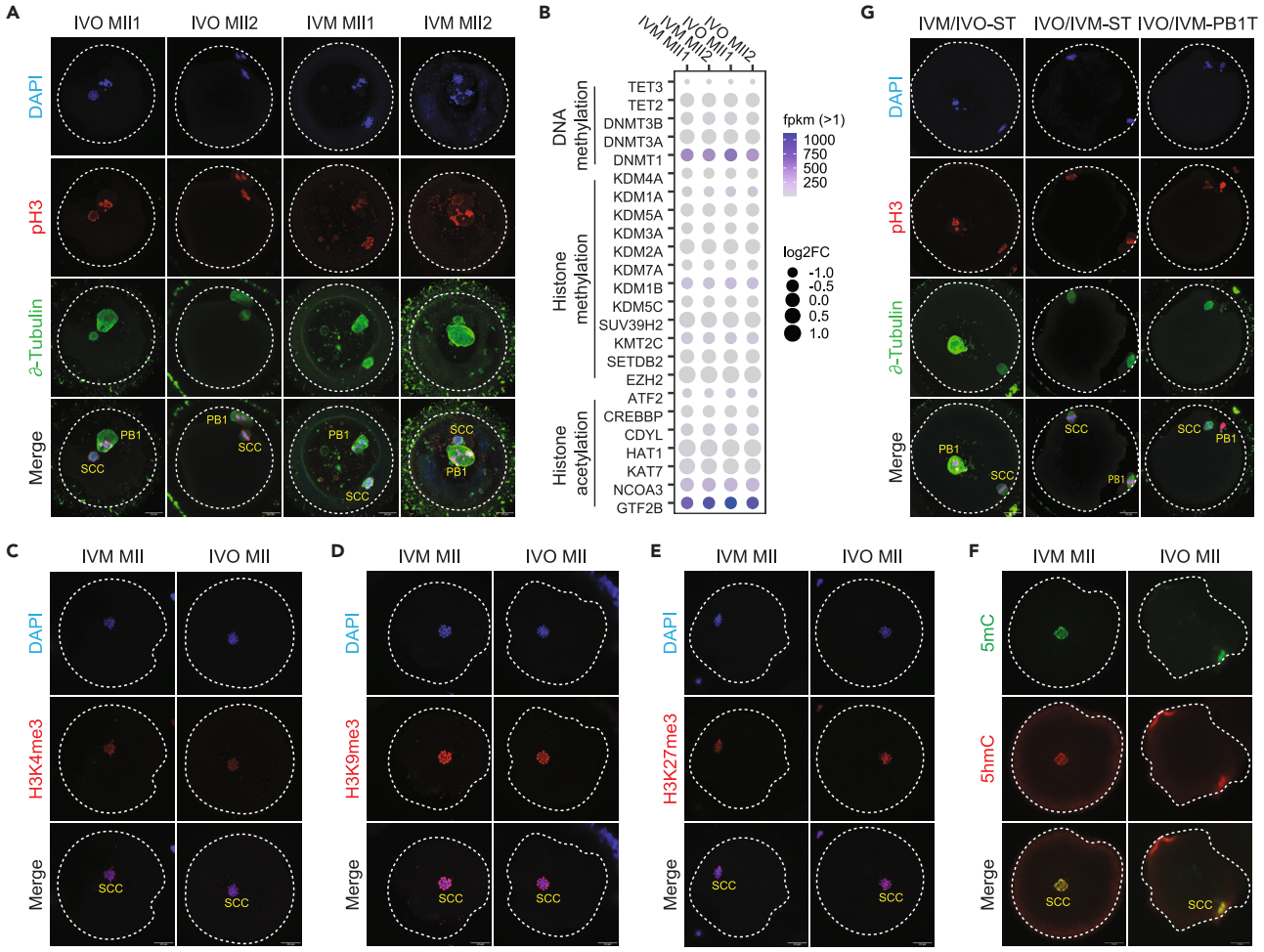

Figure 2. Genomic and epigenomic integrity analysis of monkey IVM oocytes

(A) Representative immunofluorescence image showing ∂-tubulin (green), pH3 (red), and DAPI (blue), which were used to examine the nuclear integrity in monkey IVM (n = 7) and IVO (n = 15) MII oocytes. Scale bar, 20 μm. PB1, the first polar body of the embryo. SCC, the spindle-chromosome complex of the embryos.

(B) Bubble plot showing the transcriptome expression level (based on RNA-seq data) of key epigenetic modification factors (FPKM >1) in IVM and IVO oocytes. The color of the dots indicates the FPKM of each gene, and the size of the dots indicates the log2FoldChange of expression in IVM MII oocytes compared with that in IVO MII oocytes. A single oocyte was collected for each replicate.

(C) Representative immunofluorescence image showing H3K4me3 (red) and DAPI (blue) staining in monkey IVO (n = 4) and IVM (n = 6) MII oocytes. Scale bar, 20 μm.

(D) Representative immunofluorescence image showing H3K9me3 (red) and DAPI (blue) staining in monkey IVO (n = 5) and IVM (n = 8) MII oocytes. Scale bar, 20 μm.

(E) Representative immunofluorescence image showing H3K27me3 (red) and DAPI (blue) in monkey IVO (n = 4) and IVM (n = 7) MII oocytes. Scale bar, 20 μm.

(F) Examination of DNA methylation in IVO (n = 17) and IVM (n = 18) MII oocytes. PB1 and SCCs are indicated in the figures. The oocytes are outlined by dotted white lines. Scale bar, 20 μm.

(G) Nuclear integrity of reconstructed IVM/IVO-ST (n = 2), IVO/IVM-ST (n = 3) and IVO/IVM-PB1T (n = 2) oocytes. The oocytes are outlined by dotted white lines. Scale bar, 20 μm.

reconstructed by transferring SCCs from IVO MIIs to enucleated IVM cytoplasm were called IVM/IVO-ST oocytes. The nuclear integrity of IVM/IVO-ST and IVO/IVM-ST oocytes was confirmed by the co-staining of ∂-tubulin and DNA (Figure 2G, middle). Therefore, a total of four group oocytes were included for comparison of embryonic development, namely IVO/IVM-ST, IVM/IVO-ST, IVO MII, and IVM MII.

We observed similar pronuclear formation rates and comparable cleavage rates between the four groups (Figures 3C and 3D). Almost none of the IVM- and IVM/IVO-ST-derived embryos developed to the late preimplant stage, but the rate of blastocyst formation was comparable between IVO- and IVO/IVM-ST-derived

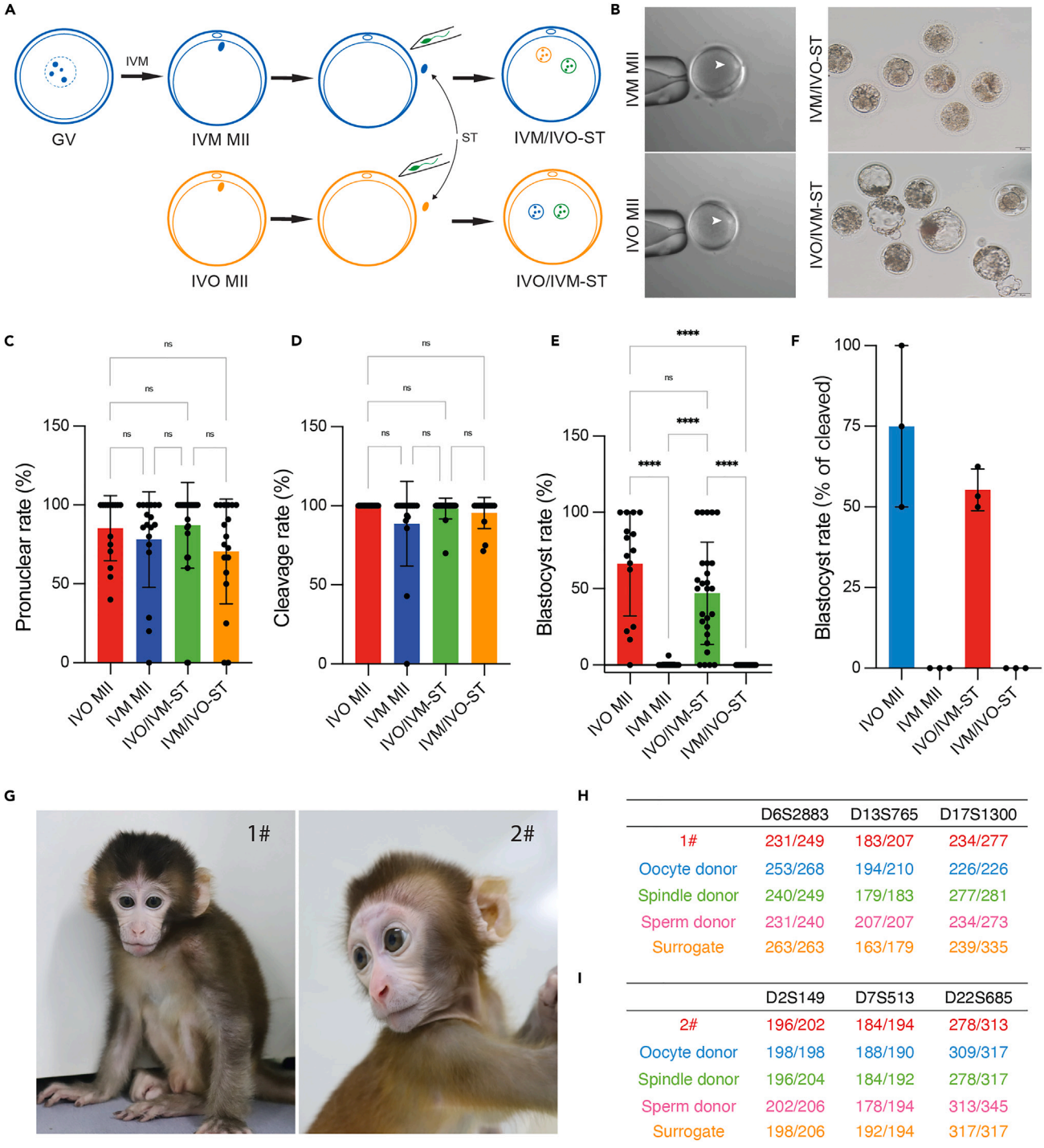

H

	D6S2883	D13S765	D17S1300
1#	231/249	183/207	234/277
Oocyte donor	253/268	194/210	226/226
Spindle donor	240/249	179/183	277/281
Sperm donor	231/240	207/207	234/273
Surrogate	263/263	163/179	239/335

I

	D2S149	D7S513	D22S685
2#	196/202	184/194	278/313
Oocyte donor	198/198	188/190	309/317
Spindle donor	196/204	184/192	278/317
Sperm donor	202/206	178/194	313/345
Surrogate	198/206	192/194	317/317

Figure 3. The live birth of IVO/IVM-ST infants

(A) Schematic illustrating of the construction of IVO/IVM-ST embryos. GV, germinal vesicle oocytes. ST, spindle transfer. The GV oocytes were initially in vitro matured to MII stage, and then their spindle-chromosome complex were transferred into enucleated IVM MII oocytes. The reconstructed oocytes were named IVO/IVM-ST and IVM/IVO-ST oocytes, respectively.

(B) Representative images of the IVM (upper left) and IVO (lower left) oocytes and IVM/IVO-ST (upper right) and IVO/IVM-ST (lower right) embryos. The SCCs are indicated by white arrowheads. Scale bar, 50 μm.

(C) The pronuclear formation rates of IVO, IVM, IVM/IVO-ST, and IVO/IVM-ST embryos after ICSI. The error bars indicate mean ± SD. The *ns* in the figure means not significant.

Figure 3. *Continued*

(D) The cleavage rates of IVO, IVM, IVM/IVO-ST, and IVO/IVM-ST embryos after ICSI. Rates were calculated based on the number of embryos with two distinct pronuclei. The error bars indicate mean ± SD. The *ns* in the figure means not significant.

(E) The blastocyst rates of embryos derived from IVO, IVM, IVM/IVO-ST, and IVO/IVM-ST oocytes. Rates were calculated based on the number of embryos with two distinct pronuclei. The data were generated using IVO and IVM oocytes from random oocyte donors. The error bars indicate mean ± SD. The *ns* in the figure means not significant. ***p-value < 0.01.

(F) Blastocyst rate of embryos derived from IVO, IVM, IVM/IVO-ST, and IVO/IVM-ST oocytes. The IVM/IVO-ST and IVO/IVM-ST embryos were reconstructed by transferring SCCs between two monkeys. The data were generated using IVO and IVM oocytes from paired oocyte donors.The error bars indicate mean ± SD.

(G) Images of the two live infants, 1# and 2#.

(H) Representative alleles of short tandem repeat analysis showing the genetic origin of infants 1# and 2#.

embryos (Figures 3B and 3E). We next performed a more careful comparison using IVM MIIs from one oocyte donor monkey and IVO MIIs from another. The ST was performed between oocytes from these paired oocyte donors. In all three replicates, the blastocyst formation rates were comparable between IVO/IVM-ST and IVO embryos (Figure 3F and Table S2).

These data together indicated that the nuclei from IVM oocytes were able to direct normal embryonic development in IVO cytoplasm before implantation. We thus concluded that the IVM cytoplasm was detrimental to oocyte competency and embryo developmental potential.

Live birth of rhesus monkeys achieved by ST

We next investigated whether IVM nuclei were able to direct full-term development after nuclear transfer. We reconstructed a total of 23 IVO/IVM-ST embryos, and 10 of them developed to the blastocyst stage (Table S3). After transferring these 10 blastocysts into the uterus of 5 surrogate mothers (2 embryos per surrogate on average), 3 of the mothers were confirmed to be pregnant by ultrasound examination (Tables 1 and S3). All of the surrogates were pregnant with singletons. Out of the three pregnancies, two resulted in live births on gestation days 178 and 175; these infants were named 1# and 2# (Figure 3G and Table 1). A stillborn infant was also obtained on day 175 and named 3# (Table 1). The genetic identities of these infants were confirmed by short tandem repeat (STR) analysis (Figures 3H, 3I, and Tables S4–S6).

These data indicated the feasibility of using the nuclei of IVM MIIs to direct the full-term development of non-human primates after ST.

Mitochondria turnover in the ST fetuses

Single nucleotide polymorphism (SNP) analysis of mitochondria confirmed the oocyte origins of the IVO/IVM-ST monkeys (Figures 4A and S3A–S3C). After sequencing the full-length mtDNA sequences of the cytoplasm donor and spindle donor, we found that there were no SNPs between these two monkeys, and concluded that no mitochondria turnover occurred in infant 1# (Figures 4A and S3A).

Pyrosequencing analysis showed a moderate mitochondria turnover rate in infants 2# and 3# (Figures 4B and 4C). We observed turnover rates of 3% and 6%, respectively, for the two SNPs in the peripheral blood of 2# (Figure 4B). The average mitochondrial turnover rates for 3# were 13.5% in the skin tissue, 7.5% in the tongue, and 5.5% in the muscle (Figures 4C and 4D). The mitochondrial turnover in ST infants can be explained by the carry-over in the ooplasm residuals during ST, as both MitoTracker staining and mtDNA copy number analysis showed comparable carry-over rate in the IVM and IVO SCCs (Figures 4E, S1D, and Table S7).

Taken together, mitochondria turnover was observed in 2 of the ST monkeys in this study, and this technical drawback needs to be overcame for the application of this IVO/IVM-ST method. But still, we obtained one ST fetus whose mitochondria were identical between the spindle-chromosome complex donor monkey and the oocyte cytoplasm donor monkey.

PB1 of IVM oocytes direct normal embryonic development in IVO oocyte cytoplasm

In addition to ST, we also performed PB1T to investigate its feasibility (Figure 5A). Here, PB1T embryos are referred to as IVO/IVM-PB1T embryos. Immunostaining of the microtubule organization of the first polar body showed that DNA was properly anchored on tubulin (Figure 2A). Epigenetic modifications, namely

Table 1. The development of IVO/IVM-ST embryos at post-implantation stage

No. of embryos transferred	No. of surrogates	Developmental stage of embryos transferred	No. of fetuses	No. of live births
10	5	blastocyst	3	2

H3K4me3, H3K9me3, H3K27me3, and DNA methylation, were also demonstrated to be comparable between the PB1s of IVM and IVO MIIs (Figures 5B–5E). The appearance of the SCCs after PB1T was similar to that of control oocytes (Figure 2G, right), indicating that the SCC organization was normal after nuclear transfer. We then performed intracytoplasmic sperm injection and observed the pre-implantation development of IVO/IVM-PB1T embryos. A total of five trials were performed, and we observed average pronuclear formation and cleavage rates of 88.6% and 96.8%, respectively (Figures 5F, 5G, and Table S8). Interestingly, the blastocyst formation rate of IVO/IVM-PB1T embryos was 43.3%, which was comparable with that of IVO/IVM-ST embryos and slightly lower than that of IVO embryos (Figures 3F and 5G).

These data indicated that the PB1 of rhesus IVM MIIs could be used for directing embryo development to at least peri-implantation stage.

DISCUSSION

Mammalian oocyte maturation from the GV stage through metaphase of the first meiosis (MI) to MII requires a complex and elaborately regulated biological system in the ovarian follicle to prepare for fertilization and further embryo development.[31,32] This process includes the maturation of both the nucleus and cytoplasm, neither of which can independently ensure the normal development of the embryo.[3,33]

In our study, the poor developmental potential of embryos generated by IVM MIIs demonstrated their incompetency. As both of the transcriptome and immunostaining results showed that the key epigenetic modification factors were comparably expressed between IVM and IVO MIIs, we speculated that the nuclear maturation was not the rate-limiting step for embryo development. However, the RNA sequencing data showed that the cytoplasmic maturation was inferior in IVM oocytes compared with that of IVO oocytes. Gene ontology analysis of the differentially expressed genes between IVM and IVO MIIs showed that the upregulated genes in IVM MIIs were mainly enriched in mitochondrial-related pathways. We therefore believe that the elevated expression of mitochondrial genes in MIIs during IVM could be attributed to the increased mtDNA copy numbers. Additionally, organelle reorganization is another important criterion for evaluating oocyte quality. Although the role of intercellular organelle reorganization during oocyte maturation is not fully understood, mitochondria have been reported to migrate from the periphery to the entire cytoplasm during human oocyte maturation from GV to MII stages.[30] The peripheral positioning of mitochondria may be related to the communication between oocytes and the surrounding somatic cells.[10] Therefore, here we concluded that the improper gene expression and the abnormal distribution of cellular organelles in IVM oocytes lead to their developmental incompetency.

The *in vitro* maturation of primate oocytes has been studied for decades since the first report by Robert G. Edwards in the 1960s. Although several thousand human babies have been born using IVM oocytes since the first IVM birth was reported by Cha et al.,[34,35] the post-implant development rate of IVM GV oocytes derived embryos is still lower than that of embryos derived from IVO oocytes.[5,8,36] Here we provided another method for synchronizing the maturation of the nucleus and cytoplasm by performing nuclear transfer. Our data showed that the nuclei of IVM oocytes were able to direct the full-term development of non-human primates, as indicated by the comparable blastocyst formation rates between IVO/IVM-ST and IVO embryos and the live birth of IVO/IVM-ST infants. Although we did not perform embryo transfer of the IVO/IVM-PB1T embryos, these embryos had a blastocyst formation rate comparable with that of IVO/IVM-ST and IVO embryos. Together, these results were consistent with a previous report, in which researchers showed that embryos reconstructed by transferring nuclei from IVM oocytes to IVO oocytes develop into blastocysts with an efficiency of 28%.[37] On the other hand, the blastocyst rates of monkey IVO/IVM-ST and IVO/IVM-PB1T embryos in this study were also comparable with that of another report, in which the authors demonstrated that the blastocyst rate of mouse GVT embryos can reached to as high as 21%.[38]

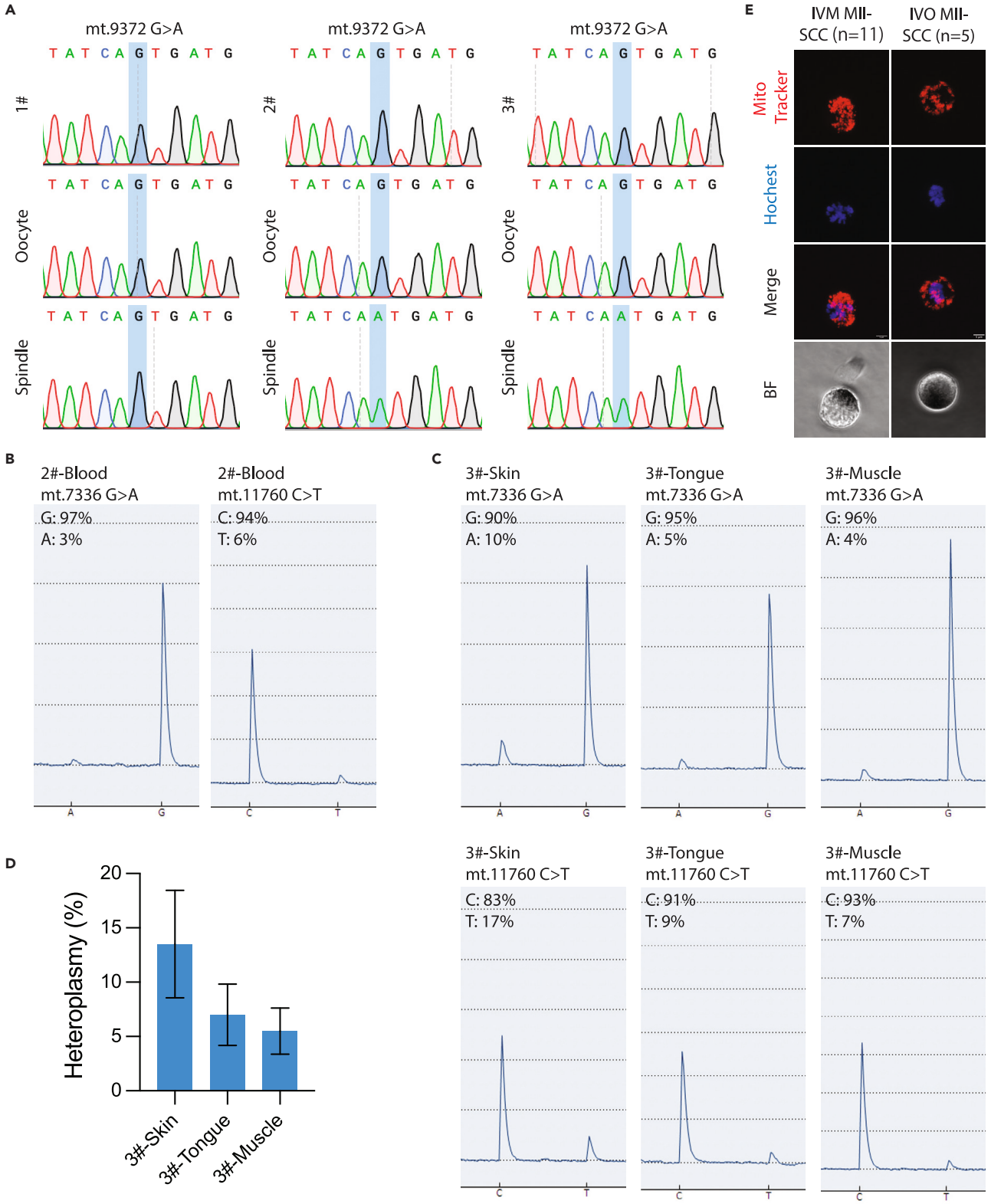

Figure 4. Pre-implant development of IVO/IVM-PB1T embryos

(A) Representative mtDNA SNPs (mt.9372). Note that there was no SNP in the cytoplasm donors and spindle donors for infant 1#.

(B) Pyrosequencing of two mtDNA SNPs (mt.7336 and mt.11760) of infant 2#. A blood sample from the infant was used.

Figure 4. *Continued*

(C) Pyrosequencing of two mtDNA SNPs (mt.7336 and mt.11760) using skin, tongue, and muscle tissues of infant 3#.

(D) Quantification of mitochondria turnover rate in different tissues (skin, tongue, and muscle) of infant 3#. The error bars indicate mean ± SD.

(E) MitoTracker staining of the SCCs from IVM and IVO oocytes. Scale bar, 5 μm.

Limitations of the study

Several concerns regarding this technique should also be noted. We only obtained 2 live infants out of 10 embryos, which is lower than the live birth rate of normal ST rhesus monkeys (4/15) reported previously.[12] In addition, we observed a high mitochondria reversal rate in two (infants 2# and 3#) of our three IVO/IVM-ST monkeys, which was mainly caused by the mitochondrial carry-over in the residual ooplasm during the ST process. The mitochondria turnover is an overt side effect of the ST and PBT technologies, and it is of great concern to researchers.[21,39] It may be possible to correct this reversion using the recently developed mitochondria genome editing technologies or mitochondria elimination method.[40–42] Nevertheless, here we provided a new way for women to preserve their fertility or increase their fertility rate by combining the IVM and nuclear transfer technologies.

STAR★METHODS

Detailed methods are provided in the online version of this paper and include the following:

- KEY RESOURCES TABLE
- RESOURCE AVAILABILITY
  - Lead contact
  - Materials availability
  - Data and code availability
- EXPERIMENTAL MODEL AND SUBJECT DETAILS
  - Animals
  - Ethics statement
- METHOD DETAILS
  - Superovulation and oocyte retrieval
  - *In vitro* maturation of immature rhesus oocytes
  - Spindle-chromosome complex transfer and PB1 transfer
  - Intracytoplasmic sperm injection, embryo culture, and embryo transfer
  - Oocyte immunofluorescence staining
  - Mitochondria distribution analysis
  - Mitochondria copy number analysis
  - Mitochondria heteroplasmy analysis
  - Short tandem repeat analysis of ST monkeys
  - Collection of monkey oocytes
  - RNA-seq for oocytes
  - RNA-seq data processing
- QUANTIFICATION AND STATISTICAL ANALYSIS
  - Statistical analyses

SUPPLEMENTAL INFORMATION

Supplemental information can be found online at https://doi.org/10.1016/j.isci.2023.107299.

ACKNOWLEDGMENTS

The authors acknowledge the members of the Non-human Primate Facility of CAS Center for Excellence in Brain Science and Intelligence Technology, especially the staff of the veterinary team for their assistance in animal experiments. This work was supported by grants from the National Key Research and Development Program of China (2022YFF0710901 to Q.S.), the National Natural Science Foundation of China Grant (31825018 and 82021001 to Q.S.), National Science and Technology Innovation 2030 Major Program 2021ZD0200900 and Lingang Lab (Grant LG202106-01-01 to Q.S. and LG202106-02-01 to Y.Z.L.), Biological Resources Program of Chinese Academy of Sciences (KFJ-BRP-005 to Q.S.), the Shanghai Municipal Science and Technology Major Project (2018SHZDZX05 to Q.S), the Strategic Priority Research Program of the Chinese Academy of Sciences (XDB32060100 to Q.S.). We especially acknowledge Prof. Qingyuan Sun for his comments and corrections to the manuscript.

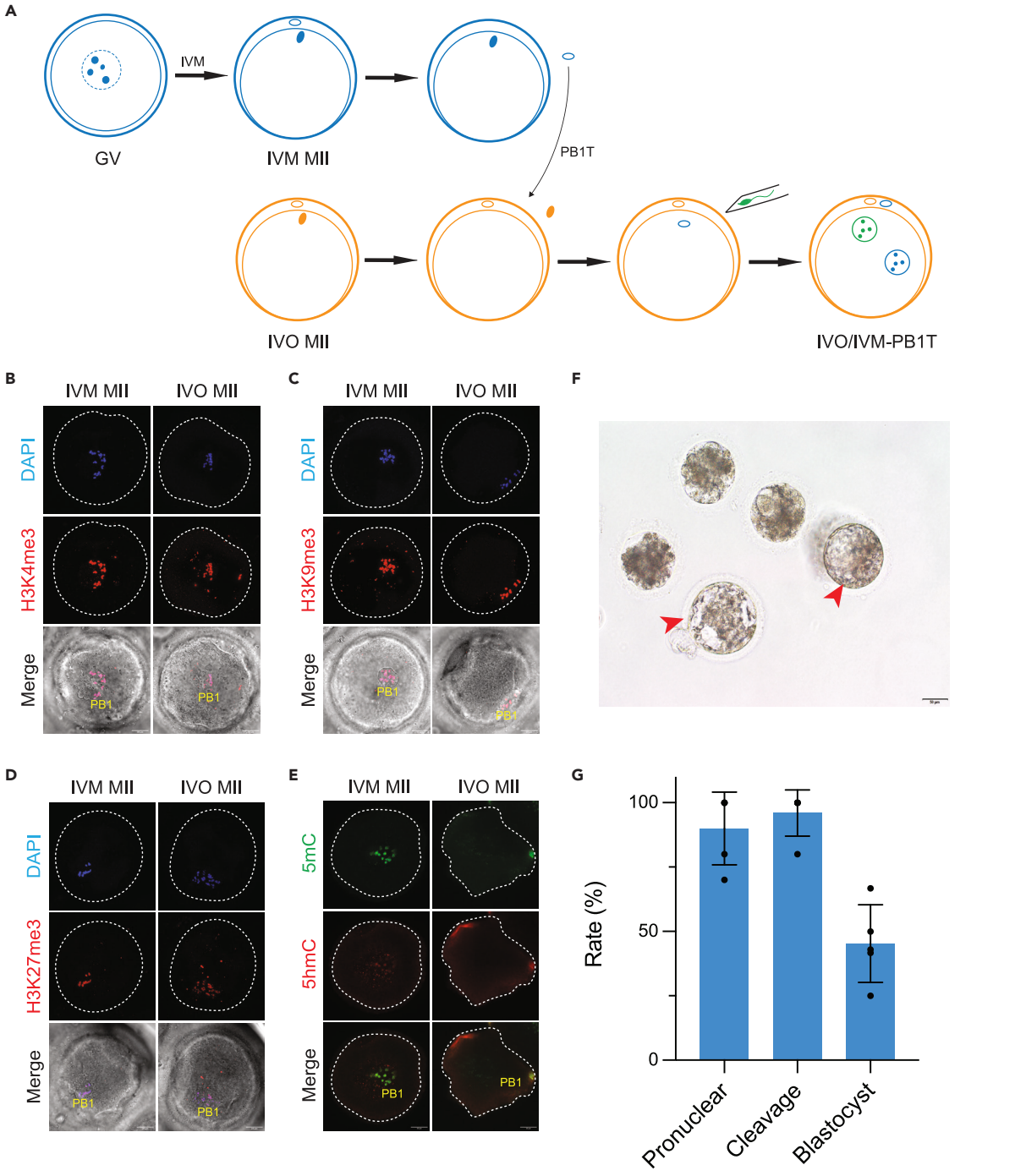

Figure 5. Pre-implant development of IVO/IVM-PB1T embryos

(A) Schematic illustration of the reconstruction of IVO/IVM-PB1T embryos.

(B) Representative immunofluorescence image showing anti-H3K4me3 (red) and DAPI (blue) staining in the first polar body (PB1) of IVM and IVO oocytes. Scale bar, 20 μm.

(C) Representative immunofluorescence image showing anti-H3K9me3 (red) and DAPI (blue) staining in the 1st PB of IVM and IVO oocytes. Scale bar, 20 μm.

(D) Representative immunofluorescence image showing anti-H3K27me3 (red) and DAPI (blue) staining in the 1st PB of IVM and IVO oocytes. Scale bar, 20 μm.

(E) Representative immunofluorescence image showing anti-5mC (green) and 5hmC (red) staining in the 1st PB of IVM and IVO oocytes. Scale bar, 20 μm.

(F) Images showing IVO/IVM-PB1T blastocysts. The blastocysts are indicated by red arrowheads. Scale bar, 50 μm.

(G) Quantification of pronuclear formation, cleavage, and blastocyst rates of IVO/IVM-PB1T embryos. The error bars indicate mean ± SD.

AUTHOR CONTRIBUTIONS

Q.S. organized this project. Z.D.L conceived the idea for the study. Z.D.L performed embryo micromanipulation, embryo transfer, molecular experiments, and data analyses. Y.Z.L. provided technical help and advice on molecular biology. C.Y.L. performed oocyte retrieval. Z.D.L. wrote the manuscript and was helped by others. All authors discussed the results, commented on the paper, and approved the final manuscript.

DECLARATION OF INTERESTS

The authors declare no competing interests.

INCLUSION AND DIVERSITY

We support inclusive, diverse, and equitable conduct of research.

Received: January 23, 2023
Revised: June 1, 2023
Accepted: July 3, 2023
Published: July 10, 2023

REFERENCES

1. Moghadam, A.R.E., Moghadam, M.T., Hemadi, M., and Saki, G. (2022). Oocyte quality and aging. JBRA Assist. Reprod. *26*, 105–122. https://doi.org/10.5935/1518-0557.20210026.

2. Gruhn, J.R., Zielinska, A.P., Shukla, V., Blanshard, R., Capalbo, A., Cimadomo, D., Nikiforov, D., Chan, A.C.-H., Newnham, L.J., Vogel, I., et al. (2019). Chromosome errors in human eggs shape natural fertility over reproductive life span. Science *365*, 1466–1469. https://doi.org/10.1126/science.aav7321.

3. Fan, H.-Y., and Sun, Q.-Y. (2019). Oocyte meiotic maturation. In The Ovary, pp. 181–203. https://doi.org/10.1016/b978-0-12-813209-8.00012-1.

4. Zhang, H., Chen, T., Wu, K., Hou, Z., Zhao, S., Zhang, C., Gao, Y., Gao, M., Chen, Z.J., and Zhao, H. (2021). Dominant mutations in CHK1 cause pronuclear fusion failure and zygote arrest that can be rescued by CHK1 inhibitor. Cell Res. *31*, 814–817. https://doi.org/10.1038/s41422-021-00507-8.

5. Practice Committees of the American Society for Reproductive Medicine and the Society for Assisted Reproductive Technology (2021). In vitro maturation: A committee opinion. Fertil. Steril. *115*, 298–304. https://doi.org/10.1016/j.fertnstert.2020.11.018.

6. De Vos, M., Smitz, J., and Woodruff, T.K. (2014). Fertility preservation in women with cancer. Lancet *384*, 1302–1310. https://doi.org/10.1016/s0140-6736(14)60834-5.

7. Segers, I., Mateizel, I., Van Moer, E., Smitz, J., Tournaye, H., Verheyen, G., and De Vos, M. (2015). In vitro maturation (IVM) of oocytes recovered from ovariectomy specimens in the laboratory: a promising "ex vivo" method of oocyte cryopreservation resulting in the first report of an ongoing pregnancy in Europe. J. Assist. Reprod. Genet. *32*, 1221–1231. https://doi.org/10.1007/s10815-015-0528-9.

8. Hatırnaz, Ş., Ata, B., Hatırnaz, E.S., Dahan, M.H., Tannus, S., Tan, J., and Tan, S.L. (2018). Oocyte in vitro maturation: A sytematic review. Turk. J. Obstet. Gynecol. *15*, 112–125. https://doi.org/10.4274/tjod.23911.

9. Walls, M.L., Hunter, T., Ryan, J.P., Keelan, J.A., Nathan, E., and Hart, R.J. (2015). In vitro maturation as an alternative to standard in vitro fertilization for patients diagnosed with polycystic ovaries: a comparative analysis of fresh, frozen and cumulative cycle outcomes. Hum. Reprod. *30*, 88–96. https://doi.org/10.1093/humrep/deu248.

10. Kirillova, A., Smitz, J.E.J., Sukhikh, G.T., and Mazunin, I. (2021). The role of mitochondria in oocyte maturation. Cells *10*. https://doi.org/10.3390/cells10092484.

11. Takeuchi, T., Gong, J., Veeck, L.L., Rosenwaks, Z., and Palermo, G.D. (2001). Preliminary findings in germinal vesicle transplantation of immature human oocytes. Hum. Reprod. *16*, 730–736. https://doi.org/10.1093/humrep/16.4.730.

12. Tachibana, M., Sparman, M., Sritanaudomchai, H., Ma, H., Clepper, L., Woodward, J., Li, Y., Ramsey, C., Kolotushkina, O., and Mitalipov, S. (2009). Mitochondrial gene replacement in primate offspring and embryonic stem cells. Nature *461*, 367–372. https://doi.org/10.1038/nature08368.

13. Paull, D., Emmanuele, V., Weiss, K.A., Treff, N., Stewart, L., Hua, H., Zimmer, M., Kahler, D.J., Goland, R.S., Noggle, S.A., et al. (2013). Nuclear genome transfer in human oocytes eliminates mitochondrial DNA variants. Nature *493*, 632–637. https://doi.org/10.1038/nature11800.

14. Zhang, J., Liu, H., Luo, S., Lu, Z., Chávez-Badiola, A., Liu, Z., Yang, M., Merhi, Z., Silber, S.J., Munné, S., et al. (2017). Live birth derived from oocyte spindle transfer to prevent mitochondrial disease. Reprod. Biomed. Online *34*, 361–368. https://doi.org/10.1016/j.rbmo.2017.01.013.

15. Tachibana, M., Amato, P., Sparman, M., Woodward, J., Sanchis, D.M., Ma, H., Gutierrez, N.M., Tippner-Hedges, R., Kang, E., Lee, H.S., et al. (2013). Towards germline gene therapy of inherited mitochondrial diseases. Nature *493*, 627–631. https://doi.org/10.1038/nature11647.

16. Palermo, G.D., Takeuchi, T., and Rosenwaks, Z. (2002). Technical approaches to correction of oocyte aneuploidy. Hum. Reprod. *17*, 2165–2173. https://doi.org/10.1093/humrep/17.8.2165.

17. Craven, L., Tuppen, H.A., Greggains, G.D., Harbottle, S.J., Murphy, J.L., Cree, L.M., Murdoch, A.P., Chinnery, P.F., Taylor, R.W., Lightowlers, R.N., et al. (2010). Pronuclear transfer in human embryos to prevent transmission of mitochondrial DNA disease. Nature *465*, 82–85. https://doi.org/10.1038/nature08958.

18. Hyslop, L.A., Blakeley, P., Craven, L., Richardson, J., Fogarty, N.M.E., Fragouli, E., Lamb, M., Wamaitha, S.E., Prathalingam, N., Zhang, Q., et al. (2016). Towards clinical application of pronuclear transfer to prevent mitochondrial DNA disease. Nature *534*, 383–386. https://doi.org/10.1038/nature18303.

19. Ma, H., O'Neil, R.C., Marti Gutierrez, N., Hariharan, M., Zhang, Z.Z., He, Y., Cinnioglu, C., Kayali, R., Kang, E., Lee, Y., et al. (2017). Functional human oocytes generated by transfer of polar body genomes. Cell Stem Cell *20*, 112–119. https://doi.org/10.1016/j.stem.2016.10.001.

20. Zhang, S.P., Lu, C.F., Gong, F., Xie, P.Y., Hu, L., Zhang, S.J., Lu, G.X., and Lin, G. (2017). Polar body transfer restores the developmental potential of oocytes to blastocyst stage in a case of repeated embryo fragmentation. J. Assist. Reprod. Genet. *34*,

563–571. https://doi.org/10.1007/s10815-017-0881-y.

21. Wang, Z., Li, Y., Yang, X., Wang, Y., Nie, Y., Xu, Y., Zhang, X., Lu, Y., Zhang, T., Liu, Q., et al. (2021). Mitochondrial replacement in macaque monkey offspring by first polar body transfer. Cell Res. *31*, 233–236. https://doi.org/10.1038/s41422-020-0381-y.

22. Goud, P.T., Goud, A.P., Qian, C., Laverge, H., Van der Elst, J., De Sutter, P., and Dhont, M. (1998). In-vitro maturation of human germinal vesicle stage oocytes: role of cumulus cells and epidermal growth factor in the culture medium. Hum. Reprod. *13*, 1638–1644. https://doi.org/10.1093/humrep/13.6.1638.

23. Brown, H.M., Dunning, K.R., Sutton-McDowall, M., Gilchrist, R.B., Thompson, J.G., and Russell, D.L. (2017). Failure to launch: aberrant cumulus gene expression during oocyte in vitro maturation. Reproduction *153*, R109–R120. https://doi.org/10.1530/REP-16-0426.

24. Younis, A.I., and Brackett, B.G. (1991). Importance of cumulus cells and insemination intervals for development of bovine oocytes into morulae and blastocysts in vitro. Theriogenology *36*, 11–21. https://doi.org/10.1016/0093-691x(91)90429-h.

25. Hazeleger, N.L., Hill, D.J., Stubbing, R.B., and Walton, J.S. (1995). Relationship of morphology and follicular fluid environment of bovine oocytes to their developmental potential in vitro. Theriogenology *43*, 509–522. https://doi.org/10.1016/0093-691x(94)00043-t.

26. Luciano, A.M., Lodde, V., Beretta, M.S., Colleoni, S., Lauria, A., and Modina, S. (2005). Developmental capability of denuded bovine oocyte in a co-culture system with intact cumulus-oocyte complexes: role of cumulus cells, cyclic adenosine 3′,5′-monophosphate, and glutathione. Mol. Reprod. Dev. *71*, 389–397. https://doi.org/10.1002/mrd.20304.

27. Zhang, L., Jiang, S., Wozniak, P.J., Yang, X., and Godke, R.A. (1995). Cumulus cell function during bovine oocyte maturation, fertilization, and embryo development in vitro. Mol. Reprod. Dev. *40*, 338–344. https://doi.org/10.1002/mrd.1080400310.

28. Pereira, N., Neri, Q.V., Lekovich, J.P., Palermo, G.D., and Rosenwaks, Z. (2016). The role of in-vivo and in-vitro maturation time on ooplasmic dysmaturity. Reprod. Biomed. Online *32*, 401–406. https://doi.org/10.1016/j.rbmo.2016.01.007.

29. Zheng, P., Si, W., Bavister, B.D., Yang, J., Ding, C., and Ji, W. (2003). 17Beta-estradiol and progesterone improve in-vitro cytoplasmic maturation of oocytes from unstimulated prepubertal and adult rhesus monkeys. Hum. Reprod. *18*, 2137–2144. https://doi.org/10.1093/humrep/deg410.

30. Liu, S., Li, Y., Gao, X., Yan, J.H., and Chen, Z.J. (2010). Changes in the distribution of mitochondria before and after in vitro maturation of human oocytes and the effect of in vitro maturation on mitochondria distribution. Fertil. Steril. *93*, 1550–1555. https://doi.org/10.1016/j.fertnstert.2009.03.050.

31. Krisher, R.L. (2013). In vivo and in vitro environmental effects on mammalian oocyte quality. Annu. Rev. Anim. Biosci. *1*, 393–417. https://doi.org/10.1146/annurev-animal-031412-103647.

32. Li, R., and Albertini, D.F. (2013). The road to maturation: somatic cell interaction and self-organization of the mammalian oocyte. Nat. Rev. Mol. Cell Biol. *14*, 141–152. https://doi.org/10.1038/nrm3531.

33. Conti, M., and Franciosi, F. (2018). Acquisition of oocyte competence to develop as an embryo: integrated nuclear and cytoplasmic events. Hum. Reprod. Update *24*, 245–266. https://doi.org/10.1093/humupd/dmx040.

34. Cha, K.Y., Koo, J.J., Ko, J.J., Choi, D.H., Han, S.Y., and Yoon, T.K. (1991). Pregnancy after in vitro fertilization of human follicular oocytes collected from nonstimulated cycles, their culture in vitro and their transfer in a donor oocyte program. Fertil. Steril. *55*, 109–113. https://doi.org/10.1016/s0015-0282(16)54068-0.

35. Sauerbrun-Cutler, M.-T., Vega, M., Keltz, M., and McGovern, P.G. (2015). In vitro maturation and its role in clinical assisted reproductive technology. Obstet. Gynecol. Surv. *70*, 45–57. https://doi.org/10.1097/OGX.0000000000000150.

36. Lin, Y.H., Tsai, C.Y., Huang, L.W., Seow, K.M., Hwang, J.L., and Tzeng, C.R. (2014). Reduced uterine receptivity for mouse embryos developed from in-vitro matured oocytes. J. Assist. Reprod. Genet. *31*, 1713–1718. https://doi.org/10.1007/s10815-014-0354-5.

37. Tanaka, A., Nagayoshi, M., Awata, S., Himeno, N., Tanaka, I., Watanabe, S., and Kusunoki, H. (2009). Metaphase II karyoplast transfer from human in-vitro matured oocytes to enucleated mature oocytes. Reprod. Biomed. Online *19*, 514–520. https://doi.org/10.1016/j.rbmo.2009.06.004.

38. Takeuchi, T., Neri, Q.V., Katagiri, Y., Rosenwaks, Z., and Palermo, G.D. (2005). Effect of treating induced mitochondrial damage on embryonic development and epigenesis. Biol. Reprod. *72*, 584–592. https://doi.org/10.1095/biolreprod.104.032391.

39. Ma, H., Van Dyken, C., Darby, H., Mikhalchenko, A., Marti-Gutierrez, N., Koski, A., Liang, D., Li, Y., Tippner-Hedges, R., Kang, E., et al. (2021). Germline transmission of donor, maternal and paternal mtDNA in primates. Hum. Reprod. *36*, 493–505. https://doi.org/10.1093/humrep/deaa308.

40. Mok, B.Y., Kotrys, A.V., Raguram, A., Huang, T.P., Mootha, V.K., and Liu, D.R. (2022). CRISPR-free base editors with enhanced activity and expanded targeting scope in mitochondrial and nuclear DNA. Nat. Biotechnol. *40*, 1378–1387. https://doi.org/10.1038/s41587-022-01256-8.

41. Adashi, E.Y., Rubenstein, D.S., Mossman, J.A., Schon, E.A., and Cohen, I.G. (2021). Mitochondrial disease: Replace or edit? Science *373*, 1200–1201. https://doi.org/10.1126/science.abg0491.

42. Fan, X.Y., Guo, L., Chen, L.N., Yin, S., Wen, J., Li, S., Ma, J.Y., Jing, T., Jiang, M.X., Sun, X.H., et al. (2022). Reduction of mtDNA heteroplasmy in mitochondrial replacement therapy by inducing forced mitophagy. Nat. Biomed. Eng. *6*, 339–350. https://doi.org/10.1038/s41551-022-00881-7.

43. Liu, Z., Li, X., Zhang, J.T., Cai, Y.J., Cheng, T.L., Cheng, C., Wang, Y., Zhang, C.C., Nie, Y.H., Chen, Z.F., et al. (2016). Autism-like behaviours and germline transmission in transgenic monkeys overexpressing MeCP2. Nature *530*, 98–102. https://doi.org/10.1038/nature16533.

44. Liu, Z., Cai, Y., Wang, Y., Nie, Y., Zhang, C., Xu, Y., Zhang, X., Lu, Y., Wang, Z., Poo, M., and Sun, Q. (2018). Cloning of macaque monkeys by somatic cell nuclear transfer. Cell *172*, 881–887.e7. https://doi.org/10.1016/j.cell.2018.01.020.

45. Liu, Z., Cai, Y., Liao, Z., Xu, Y., Wang, Y., Wang, Z., Jiang, X., Li, Y., Lu, Y., Nie, Y., et al. (2019). Cloning of a gene-edited macaque monkey by somatic cell nuclear transfer. Natl. Sci. Rev. *6*, 101–108. https://doi.org/10.1093/nsr/nwz003.

STAR★METHODS

KEY RESOURCES TABLE

REAGENT or RESOURCE	SOURCE	IDENTIFIER
Antibodies		
Anti-∂-tubulin	abcam	ab80779
anti-phosphate H3	abcam	ab5176
anti-H3K4me3	abcam	ab8580
anti-H3K9me3	abcam	ab8898
anti-H3K27me3	CST	9733S
anti-5mC antibody	Millipore	NA81
anti-5hmC	Active Motif	39769
Alexa Fluor 488 anti-mouse IgG	Jackson ImmunoResearch	115-545-003
Alexa Fluor Cy3 anti-rabbit IgG	Jackson ImmunoResearch	111-165-003
MitoTracker™ Red CMXRos - Special Packaging	Invitrogen™	M7512
Hoechst 33342	Beyotime	C1026
DAPI	Beyotime	C1005
Bacterial and virus strains		
HVJ-E	Cosmo Bio Co. Ltd	808920
Biological samples		
Rhesus germinal vesicle oocytes (GV)	This paper	N/A
Rhesus *in vitro* matured oocytes (IVM MII)	This paper	N/A
Rhesus *in vivo* matured oocytes (IVO MII)	This paper	N/A
Chemicals, peptides, and recombinant proteins		
Chorionic Gonadotrophin Human	Sigma	CG10-10VL
Recombinant Human Follitropin	Merk Serono	S20130055(75IU)
Heparin sodium salt	Shanghai Sanjie Bio Co. Ltd	091201
CMRL-1066 medium	Gibco	11530-037
Cytochalasin B	Sigma	C6762
Hamster embryo culture medium 9 (HECM-9)	This paper	Home made
HEPES-buffered Tyrode's lactate medium (TH3)	This paper	Home made
Fetal bovine serum	Gibco	30044333
Sodium pyruvate	Sigma	P5280-25G
Glutamine	Sigma	G8540-25G
Calcium lactate	Sigma	C8356-250G
MEM NEAA	Gibco	11140050
β-Estradiol	Sigma	E2758
Paraformaldehyde (PFA)	Sigma	P6148
Phosphate buffered saline (PBS)	Gibco	10010023
Distilled water	Gibco	15230-162
Triton-X-100	Beyotime	ST795
Donkey serum	Sigma-Aldrich	D9663
Bovine serum albumin	Sigma	A1933
Tween-20	Beyotime	ST825-100ml
Hydrochloric acid (HCl)	Sinopharm	10011028

(*Continued on next page*)

Continued

REAGENT or RESOURCE	SOURCE	IDENTIFIER
Critical commercial assays		
REPLI-g Single Cell Kit	Qiagen	150343
QIAcuityTM Probe PCR Kit	QIAGEN	250101
QIAcuity Nanoplate 26k 24-well Kit	QIAGEN	250001
QIAcuity Digital PCR System QIAcuity One	QIAGEN	911021
TIANamp Genomic DNA Kit	Tiangen	DP304-03
Phanta Max Super-Fidelity DNA Polymerase	Vazyme	P505-d1
Takara LA Taq	Takara	RR002A
Deposited data		
Oocyte RNA-seq	GEO	GSE233232
Experimental models: Organisms/strains		
Rhesus monkeys (*Macaca Mulatta*)	Sheshan, Shanghai	N/A
Oligonucleotides		
Primers for mtDNA SNPs identification: 278F, catgcagttgttgatcgcaccta; 278R, ggtttggcaagagtgggtt; 4061F, acaaccacaatcttcctaggcaca; 4061R, ggggaatgctggagattgcg; 4591F, cctgagaatccaaacttctccgtg; 4591R, agcatcctgatagtaggttgttgg; 5803F, ctgcaaacacctactctgcatcaa; 5803R, ggctcagggcagtgcctatga; 6040F, tcataggcactgccctgagcc; 6040R, gcggctaggactggtagagagag; 6988F, ataatcattgcaatccccaccggt; 6988R, gatggtgaaggatgggtcgttg; 8680F, acccctttctcaaccccaacaatc; 8680R, tggtaggaggtgggctagggag; 9543F, catagttaaacccagtccctggcc; 9543R, tcggagatggtgaagggtgcttc; 10051F, accacaggcttccacggac; 10051R, gggaggtttgttgtttgaatggct; 11530F, gagaccactctcattcctaccct; 11530R, tgttttctcgtgtgaaggggggg; 13628F, cccttcctcacaggcttctactcc; 13628R, gttagtggtgtggttggttgtgtg; 15129F, ggactccaaccataactaacggca; 15129R, gctgtcaatggcgtatcctcctc; 16038F, cactatcggccaagtagcatccat; 16038R, gcatccgtggtgaggaggattat	This paper	N/A
Primers for full-length mtDNA amplification: 2080F, agacactaggaaaaaaccttatagagagagt; 2079R, aaagagctgtccctctttagactagc	This paper	N/A
Software and algorithms		
ABI PRISM 3730 genetic analyzer	ABI	N/A
ImageJ	N/A	https://imagej.nih.gov/ij/
fastp (version 0.23.2)	N/A	https://github.com/OpenGene/fastp
SAMtools (version 1.15.1)	N/A	https://github.com/samtools/samtools
featureCounts (version 2.0.1)	N/A	https://subread.sourceforge.net/featureCounts.html
Bowtie2 (version 2.4.5)	N/A	https://bowtie-bio.sourceforge.net/bowtie2/index.shtml
R (version 4.2.1)	N/A	https://www.r-project.org
GraphPad Prism 9 (Version 9.1.1)	N/A	N/A
SnapGene (Version 4.3.6)	N/A	N/A
Other		
Agilent 2100 bioanalyzer	Agilent Technologies	N/A
Novaseq 6000 sequencer	Illumina	N/A
Glass bottom culture dish	Fluoro Dish	FD3510-100

(*Continued on next page*)

Continued

REAGENT or RESOURCE	SOURCE	IDENTIFIER
Adhesion Microscope Slides	CITOTEST	188105W
Piezo impact drive system	Prime Tech	N/A
Oosight imaging system	Cri	N/A
Laser system	Hamilton Thorne	N/A
P97 micropipet puller	Sutter Instrutment	N/A
Inverted microscope	Olympus	IM-73
Syringe IM 9B	Narishige	N/A
Syringe CellTram vario	Eppendorf	N/A
FV3000	Olympus	N/A
Fluoview FV10i	Olympus	N/A

RESOURCE AVAILABILITY

Lead contact

Further information and requests for resources and reagents should be directed to and will be fulfilled by the lead contact, Qiang Sun (qsun@ion.ac.cn).

Materials availability

This study did not generate new reagents and all reagents were commercially purchased and used as received.

Data and code availability

- The RNA-seq datasets of GV, IVM MIIs and IVO MIIs were deposited to the Gene Expression Omnibus (GEO) repository with the accession number of GSE233232. The accession number is also listed in the key resources table. The dataset is declared to be publicly accessible.
- This paper did not generate original code.
- Any additional information required to reanalyze the data in this paper is available from the lead contact upon request.

EXPERIMENTAL MODEL AND SUBJECT DETAILS

Animals

Monkeys used in this research were from the non-human primate facility of the Center for Excellence in Brain Science and Intelligence Technology, Shanghai, China.

Ethics statement

All animal procedures followed the guidelines of the Animal Use and Care Committees at the Shanghai Institute of Biological Science, Chinese Academy of Sciences, and Institute of Neuroscience, CAS Center for Excellence in Brain Science and Intelligence Technology. The application approved by the committees was entitled "Routine operation of assisted reproduction and sample collection of non-human primate in Suzhou Non-human Primate Research Facility" (ION-2019043).

METHOD DETAILS

Superovulation and oocyte retrieval

Hormone-stimulated oocyte superovulation was performed as we previously reported.[43–45] Monkeys were treated with recombinant human follitropin every 2 days for about a week in total, then one shot of human chorionic gonadotropin (hCG) was injected on day 11. Oocytes in the follicles were aspirated at about 36 h after the hCG injection. The cumulus cells surrounding the oocytes were denuded by a brief hyaluronidase treatment and gentle pipetting. The denuded oocytes were then divided into metaphase II-arrested (MII), metaphase I-arrested (MI), and germinal vesicle (GV) stages according to the appearance of the GV and first

polar body (PB1). All of the oocytes were then put into modified 1066 supplemented with β-estradiol for further maturation.[29] The MII and GV oocytes were selected for further application.

In vitro maturation of immature rhesus oocytes

To capture the low-quality oocytes for studying how to promote developmental efficiency, we adopted a previously reported modified 1066 maturation medium.[29] In detail, the commercial CMRL-1066 medium was supplemented with 10% fetal bovine serum, 40 mg/L sodium pyruvate, 150 mg/L glutamine, 550 mg/L calcium lactate, and β-Estradiol. On the other hand, the cumulus cell-denuded GV stage oocytes were collected and cultured in this modified 1066 maturation medium for 24 h. The maturation medium was prepared freshly on the day of oocyte collection.

Spindle-chromosome complex transfer and PB1 transfer

Oocytes were placed in a pre-equilibrated modified HEPES-buffered TALP medium (TH3) containing 5 μg/mL cytochalasin B (a cytoskeletal inhibitor) covered with paraffin oil on a glass-bottomed dish. The dish containing oocytes was placed under the Oosight Imaging System for spindle-chromosome complex (SCC) removal as we previously reported.[44,45] The SCCs were carefully removed using a blunt-end micropipette and placed in a new TH3 drop for the transfer. Then the enucleated oocytes were transferred to pre-equilibrated hamster embryo culture medium-9 (HECM-9) and incubated at 37°C in 5% CO_2 until all of the oocytes were enucleated. Before the SCC introduction, a small slit in the zona pellucida was created by laser irradiation. Then SCCs briefly treated with the inactivated hemagglutinating virus of Japan envelope (HVJ-E) were introduced into the perivitelline space of the enucleated oocytes using a homemade beveled micropipette. After the SCCs were fused with the enucleated oocytes (usually within 1 h), the reconstructed oocytes were fertilized by intracytoplasmic sperm injection.

The procedure for the PB1 transfer (PB1T) was performed similarly to that of SCC transfer (ST), except that the PB1s were removed from the donor oocytes using a beveled micropipette rather than a blunt-end micropipette.

Intracytoplasmic sperm injection, embryo culture, and embryo transfer

Intracytoplasmic sperm injection was performed as we previously reported.[43] Briefly, an oocyte was held by a holding pipette while the zona pellucida and cytoplasm membrane were penetrated by a piezo-driven injection pipette. After the penetration, a single immobilized spermatozoon was released into the cytoplasm.

After intracytoplasmic sperm injection, the embryos were transferred into the pre-warmed HECM-9 medium at 37°C in 5% CO_2 for further culture. The culture medium was changed with fresh HECM-9 medium supplemented with 5% fetal bovine serum on the third day after fertilization, and the medium was then changed every 2 days until the embryos developed to the blastocyst stage.

The blastocysts were then transferred to the oviducts of surrogates. The menstrual cycles of the surrogates were recorded daily, and the females with a fresh stigma of ovulation on their ovaries were used as recipients in this study.

Oocyte immunofluorescence staining

For immunostaining, IVM MII, IVO MII, and GV oocytes were collected and fixed with 4% paraformaldehyde (PFA) for 30 min at room temperature. The oocytes were then washed with PBS (phosphate-buffered saline) containing 0.1% bovine serum albumin (BSA) and permeabilized by incubating in 0.5% Triton X-100 in PBS for 30 min. After the permeabilization step, the specimens were transferred to PBS containing 10% donkey serum and blocked for 1 h.

Next, the specimens were incubated with primary antibody overnight at 4°C. Specimens were then washed in PBS containing 0.1% BSA 3 times, 10 min each. After washing out the primary antibodies, the oocytes were incubated with the second antibodies for 4 h at 37°C. The oocytes were washed in PBS containing 0.1% BSA another three times, 10 min each. The stained oocytes were finally placed into a new drop of PBS, covered with paraffin oil in a glass-bottomed dish (WPI, FD3510-100), and imagined by an FV3000 (Olympus). Z stack confocal imaging was performed with a 1-μm interval.

The final concentrations of antibodies and DAPI used in this study were as follows: anti-∂-tubulin (1:200, abcam, ab80779), anti-phosphate H3 (1:100, abcam, ab5176), anti-H3K4me3 (1:1000, abcam, ab8580), anti-H3K9me3 (1:200, abcam, ab8898), anti-H3K27me3 (1:1000, CST, 9733S), Alexa Fluor 488 anti-mouse IgG (1:5000, Invitrogen), Alexa Fluor Cy3 anti-rabbit IgG (1:5000, Invitrogen), and DAPI (1:5000).

For the immunostaining of 5mC and 5hmC, IVM MII- and IVO MII-derived 1-cell stage embryos were collected and fixed in 4% PFA overnight at 4°C and permeabilized with 0.5% Triton X-100 in PBS for 1 h. After three washes in PBS containing 0.05% Tween-20, all samples were treated with 4 M HCl for 10 min and fully rinsed again with 0.05% Tween-20. After three washes, samples were blocked in 1% BSA overnight at 4°C. The embryos were next incubated with anti-5mC antibody (1:200, Millipore, NA81-50UG) and anti-5hmC (1:200, Active Motif, 39769) at 25°C for 3 h. Then they were washed with 0.1% BSA in PBS three times, 10 min each. After washing, the samples were incubated with Alexa Fluor 488 anti-mouse IgG (1:1000, Invitrogen) and Alexa Fluor Cy3 anti-rabbit IgG (1:1000, Invitrogen) at 25°C for an additional 8 h. Finally, the samples were washed with 0.1% BSA in PBS and imaged by an FV3000.

Mitochondria distribution analysis

Whole oocytes and SCCs were collected and stained with MitoTracker (250 nM, Life Technologies), a dye for mitochondrion staining, and Hoechst 33342 (1 μg/mL, Sigma) for DNA staining, for 30 min at 37°C in 5% CO_2, and then washed with pre-warmed fresh HECM-9 medium three times, 3 min each. After washing, oocytes and SCCs were transferred to a 3.5-cm glass-bottomed dish for confocal imaging. Laser scanning was performed with a 1-μm Z-axis interval by Fluoview FV10i (Olympus).

Mitochondria copy number analysis

Whole IVM MII oocytes (n = 11), IVO MII oocytes (n = 12), and GV (n = 15) oocytes (all stripped of cumulus cells) and SCCs of IVM MII oocytes (n = 26) and IVO MII oocytes (n = 23) were carefully washed with PBS containing 0.1% BSA and transferred to PCR tubes containing 3.5 μL PBS. Each tube was placed with a single sample. After a short spin, 3 μL freshly prepared Buffer D2 (DLB: DTT = 11:1, QIAGEN, 150343) was added to each tube. Then the samples were incubated in PCR Amplifier at 65°C for 15 min and held at 10°C. Finally, 3 μL Stop Solution was added to each PCR tube resulting in a total volume of 10 μL lysate per sample. Before the digital PCR reaction was performed, the oocyte lysates were diluted 20 times, while the SCC lysates were not diluted.

The digital PCR reaction mixes were prepared according to the number of reactions needed. The components (40 μL) of each reaction mix were10 μL 4X Probe PCR Master Mix (provided in the QIAcuity Probe PCR Kit, QIAGEN, 250101), 0.8 μL forward primer (40 pmol/μL), 0.8 μL reverse primer (40 pmol/μL), 0.8 μL Taqman Probe (20 pmol/μL), 1 μL DNA template, and 26.6 μL RNase-free water. The reaction mix, which contained all components except the template, was vortexed and the appropriate volume was dispensed into the wells of a standard PCR plate. Then, template DNA was added to each well containing the reaction mix. Next, the contents of each well of the standard PCR plate were transferred to the wells of a nanoplate, which was sealed using the QIAcuity Nanoplate Seal provided in the QIAcuity Nanoplate 26k 24-well Kit (QIAGEN, 250001). The nanoplate was then placed into the QIAcuity instrument (QIAcuity Digital PCR System QIAcuity One, QIAGEN, 911021) for digital PCR. The thermal cycling conditions for digital PCR were a 2-min initial heat activation at 95°C and a two-step cycle (40 cycles): 15 s at 95°C (denaturation) and 30 s at 59°C (combined annealing and extension).

The 26k chip in the QIAcuity Nanoplate 26k 24-well Kit is composed of 24 small chip arrays, and each chip array has a total reaction system of 40 μL and 26,000 points. The software automatically calculates the copy number of the target gene in the reaction system per μL according to the copy number. The concentration of each sample was obtained by multiplying by the reaction volume (40 μL). The total mitochondria copy number was obtained by multiplying the volume of lysate (10 μL) and the dilution factor (20 for oocytes and 1 for SCCs).

Mitochondrial DNA (mtDNA) copy number analysis was performed by digital PCR using a target template spanning nt13523–nt13606 of the monkey mitochondrial genome. The primer sequences were CGAAG CCACAAACACGTCATAT (Forward) and GTGCTGTAGGCGCTTGTTAGG (Reverse). The TaqMan probe sequence was 5′ FAM-TGAGCCCTATTTATTACTCTC-MGB 3′ (Invitrogen).

Mitochondria heteroplasmy analysis

Mitochondria heteroplasmy analysis was performed by Sanger sequencing and pyrosequencing. The blood samples of infants 1# and 2#, the oocyte donor, and the nuclear donor were prepared for DNA extraction using the TIANamp Genomic DNA Kit (Tiangen, DP304-03). For the 3# ST monkey, genomic DNA was extracted from the skin, tongue, and muscle.

For Sanger sequencing, the monkey mitochondria genome (whole length 16,756 bp) was amplified with the Phanta Max Super-Fidelity DNA Polymerase (Vazyme, P505-d1). The PCR reaction mix consisted of 9 μL distilled water, 12.5 μL 2X Phanta Buffer, 0.5 μL dNTP Mix, 0.5 μL polymerase, 1 μL forward primer (10 μM), 1 μL reverse primer (10 μM), and 0.5 μL DNA template. The thermal cycling condition for PCR was a 5-min heat activation at 95°C, a 3-step cycle (35 cycles of a 30-s denaturation at 95°C, 30-s annealing at 58°C, and a 1-min extension at 72°C), an extra extension at 72°C for 5 min, and a final hold at 16°C. The time for extension was adjusted according to the length of the target sequence.

The full-length mitochondria genome amplification and sequencing were performed as previously reported.[39] The PCR reaction system contained 2.5 μL 10X buffer, 2.5 μL $MgCl_2$, 4 μL dNTP, 0.25 μL LATaq (Takara, RR002A), 1 μL forward primer, 1 μL reverse primer, 0.5 μL DNA template, and 13.25 μL distilled water. PCR was performed as follows: 1 min at 94°C, 10 s at 98°C for denaturation, 17 min at 68°C for annealing and elongation (30 cycles of denaturation, annealing, and elongation), 10 min for repair extension at 72°C, and a final hold at 10°C. The PCR products were then sequenced.

The mitochondrial genomes (mtDNA) of infant 1#, 2# and 3# and their cytoplasm and SCC donor monkeys were separately amplified using the following primer pairs: 278F/3307R, 3307F/5803R, 6040F/8680R, 8680F/10051R, 10051F/11530R, 11530F/13628R, 13628F/15129R, 15129F/278R, and 15129F/16038R. For infants 2# and 3#, two SNPs for each infant were selected for subsequent pyrosequencing. The SNPs used for detecting the mitochondria heteroplasmy of 2# and 3# were mt.7336 G>A and mt.11760 C>T. The primers used for amplification of mt.7336 G>A were TAGGCTGGTTCTTCGAATGTGTGA (6988-2BR) and CAACCCCTTACTAACCTAGA (6988-2FS). The pyrosequencing primer for mt.7336 G>A was ACATGATCTGAGAGGCCTTTGCTT. The primers for amplification of mt.11760 C>T were 6988-2BR: TTGAAGTCCTCGGGACAGTAGT (11530-1BR) and CCTAGCCAATTCAAACT (11530-1FS). The pyrosequencing primer for mt.11760 C>T was TCCAAACCCCCTGAAGCT. The PCR amplification system consisted of 2 μL dNTP Mix, 5 μL taq buffer (with $MgCl_2$), 0.5 μL taq polymerase, 2 μL forward primer, 2 μL reverse primer, 1 μL DNA template, and 37.5 μL distilled water to bring the final volume up to 50 μL. The PCR cycle was as follows: 95°C for 5 min; 35 cycles with denaturation at 94°C for 30 s, annealing at 55°C for 30 s, and elongation at 72°C for 50 s; 1 cycle at 72°C for 8 min.

Pyrosequencing was performed on the PyroMark Q96 ID platform according to the manufacturer's instructions (QIAGEN). Quantification of the heteroplasmy levels of variant mt.7336 G>A and mt.11760 C>T was achieved using the allele frequency quantification (AQ) function in PyroQ-AQ software to compare the status of nucleotides at the relevant position.

Sequence alignments were performed using SnapGene (Version 4.3.6).

Short tandem repeat analysis of ST monkeys

Short tandem repeat (STR) analysis was performed as described previously.[21,44,45] Whole genomic DNA was extracted from the ear tissue of monkeys 1# and 2#. The blood samples of the oocyte donor monkey, SCC donor monkeys, sperm donor monkeys, and surrogates were drawn for whole genome extraction. Locus-specific primers labeled with a fluorescent dye (FAM/HEX/TMR), were used for PCR amplification in batches. FAM-, HEX-, or TMR-labeled STR amplicons were diluted and mixed with the internal size standard ROX500 and deionized formamide, followed by capillary electrophoresis on an ABI PRISM 3730 genetic analyzer to obtain the raw data. Sequencer-generated raw data were analyzed with the program Gene Marker 2.2.0, which produces wave plots, Excel documents (including information such as size and genotype), and DNA profiles.

Collection of monkey oocytes

The GV oocytes, *in vitro* matured MII oocytes (IVM MIIs) and *in vivo* matured MII oocytes (IVO MIIs) were collected for total RNA extraction and sequencing. The zona pellucida and surrounding cumulus cells of

these oocytes were removed with the treatment of acid Tyrode's solution. Next, the oocytes were thoroughly washed in prewarmed PBS containing 0.1% BSA using mouth pipette. Then, the GV, IVM MII and IVO MII oocytes were separately transferred into each tube containing freshly prepared lysis buffer. Here, 5 oocytes were collected for each replicate of the GV and IVO MII group, 3 and 4 oocytes were collected for each replicate of the IVO MII group. Finally, the samples were fast frozen in liquid nitrogen.

RNA-seq for oocytes

The oocytes were lysed in 72°C and then put back on ice. Then the samples were spined down and reverse transcribed to cDNA based on polyA tail. Switch the template at 5′ end of the RNA and amplify the full-length cDNA by PCR. Quality control of the amplification products were performed using Agilent 2100 bioanalyzer instrument (Agilent High Sensitivity DNA Reagents). Then, the library was constructed following the Tagmentation-based library construction protocol. The double stranded PCR products were purified using the Agencourt AMPure XP-Medium kit and quantified by Agilent 2100 bioanalyzer. Next, the DNA were heat denatured and circularized by the split oligo sequence. The qualified single strand circle DNA were formatted as the final library. Finally, the library was amplified to make DNA nanoballs (DNB) which were loaded into the patterned nanoarray and the reads of paired-end 100 bases were generated in the way of sequenced by combinatorial Probe-Anchor Synthesis (cPAS).

RNA-seq data processing

Raw reads of the RNA-seq data were trimmed using trim_galore (version 0.6.7) with default parameters. Then the clean reads were aligned to *Macaca fascicularis* genome (macFas5) using bowtie2 (version 2.4.5) with default parameters. The resulted SAM files were converted to BAM files and indexed using samtools (version 1.15.1). The raw counts of each sample were obtained using featureCounts (version 2.0.1) with default parameters. The differentially expressed genes were identified using DESeq2. The heatmap illustration showing DEGs between GV, IVM oocytes and IVO oocytes were performed using ComplexHeatmap in R. The Pearson's correlation between biological replications was calculated using the FPKM by the *cor* function in R.

QUANTIFICATION AND STATISTICAL ANALYSIS

Statistical analyses

The pronuclear formation, embryo cleavage, and blastocyst formation rates were analyzed using Kruskal-Wallis one-way analysis of variance by ranks. All of the statistical analyses were performed using GraphPad Prism 9 (Version 9.1.1).